Catastrophic Thinning of Dielectric Elastomers

G. Zurlo* and M. Destrade
School of Mathematics, Statistics and Applied Mathematics, NUI Galway, University Road, Galway, Ireland

D. DeTommasi and G. Puglisi
Dipartimento di Scienze dell' Ingegneria Civile e dell' Architettura, Politecnico di Bari, Via Re David 200, 70125 Bari, Italy

(Received 6 October 2016; published 15 February 2017)

We provide an energetic insight into the catastrophic nature of thinning instability in soft electroactive elastomers. This phenomenon is a major obstacle to the development of giant actuators, yet it is neither completely understood nor modeled accurately. In excellent agreement with experiments, we give a simple formula to predict the critical voltages for instability patterns; we model their shape and show that reversible (elastic) equilibrium is impossible beyond their onset. Our derivation is fully analytical, does not require finite element simulations, and can be extended to include prestretch and various material models.

DOI: 10.1103/PhysRevLett.118.078001

Consider a thin dielectric plate with conducting faces: when will it break if a voltage is applied? If it is rigid, it will break once its dielectric strength is overcome by the voltage. However, what if it is highly stretchable, like the elastomers used for soft actuators, stretchable electronics, or energy harvesters? The precise answer to that question is not known. Experiments show that it will break when highly localized thinning deformations occur and, furthermore, that this process is *catastrophic*, as the deformations can neither be controlled nor restrained once they have started.

Here, we unveil the physical meaning of catastrophic thinning, based on energy minimization arguments; we derive a unifying and simple formula giving very accurate predictions of the voltage thresholds for the *creasing instability* (one-side constrained plates, with a compliant electrode on one face and a rigid electrode on the other face) and the *pull-in instability* (unconstrained plates with fully compliant electrodes glued on both faces); we calculate the shape of the instability patterns at their onset, and we show that they are not sustainable but that they give the path to final breakdown; we generalize the results to include prestretch.

Typically, thin dielectric elastomers are highly deformable (isotropic, incompressible) polymeric or silicone electroelastic films, brushed with conductive carbon grease [1]. With an applied electric field, the attractive Coulomb forces between the electrodes compress the thickness of the film, which expands in its plane. At first, the rectangular film deforms homogeneously into another rectangle, until a *critical voltage* is reached. Then a sudden, irreversible, and nonhomogeneous thinning localization occurs (usually accompanied by a spark and a popping sound [2]), anticipating the dielectric breakdown of the film, forming holes, and significantly reducing its capacitance (Fig. 1).

Call E the following nondimensional measure [4] of the electric field:

$$E = \sqrt{\frac{\epsilon}{\mu}}\frac{V}{h}, \tag{1}$$

and E_c its critical value. Here, V is the applied voltage, ϵ is the dielectric permittivity of the elastomer, μ its initial shear modulus, and h its initial thickness. For unconstrained plates, experiments [5] give an E_c in the range 0.678–0.686 at the onset of pull-in instability, corresponding to a contraction of 30%–34% in the layer's thickness. For one-side constrained plates, experiments [6] reveal that $E_c \simeq 0.85$. Finally, extensive experimental studies document that dead loads (for unconstrained films) and

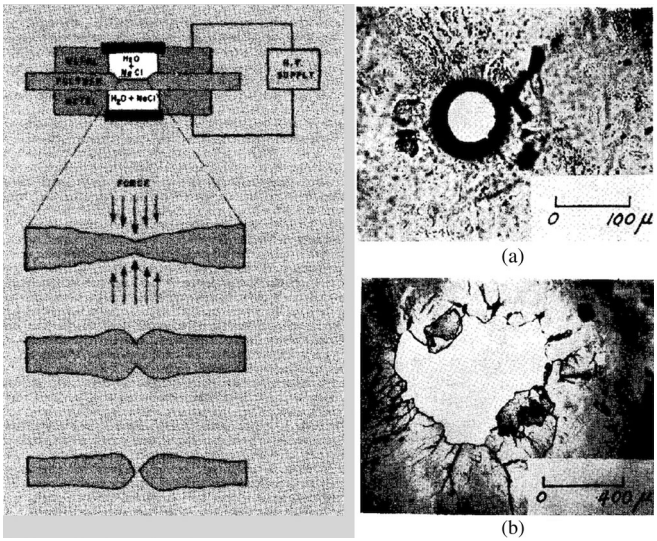

FIG. 1. (Right panels a,b) First recorded experimental evidence of catastrophic localization of thinning deformations (pull-in instability). Reprinted from [3], with the permission of AIP Publishing. (Left panel) Sketch of the experimental setting and qualitative description of the localizations.

prestretch (for one-side constrained films) play a beneficial role in delaying the onset of instabilities [7–9].

However, despite the abundance of experimental data, the critical values of the electric field to date have not been predicted by theory in an entirely satisfying manner. Many papers establish a connection between pull-in and snap-through instabilities for unconstrained films [4] using the so-called Hessian method, but when dead loads are applied, these predictions fail to account for the actual delay of instability, a key factor for technological applications [7]. Indeed, dead loads can suppress snap-through instability, but not the catastrophic thinning leading to failure. For unconstrained films, there were attempts at introducing linearized [10–13] and nonlinear [14] inhomogeneous bifurcation modes on top of the homogeneous deformation, but they require lengthy calculations, do not explain the catastrophic nature of localized deformations, and do not quantify the beneficial effects of prestretch. The situation is even worse for one-side constrained films. So far, electro-creasing has been studied only with entirely numerical methods based on finite element method (FEM) simulations: in the absence of prestretch, they lead to an estimate of $E_c \simeq 1.03$, which is more than 20% off the experimental mark [6] of $E_c \simeq 0.85$. There are no theoretical predictions available when prestretch is applied.

Our analysis [15] does not require the machinery of classical bifurcation methods. It provides a new paradigm for understanding electromechanical instability, which we find corresponds to a threshold where the electroelastic energy does not possess minimizers in a general class of homogeneous and nonhomogeneous deformations. For both unconstrained and constrained films, with and without prestretch and for a quite general class of incompressible materials, we obtain the following simple *unifying formula* for the critical electric field:

$$E_c = \frac{2}{\sqrt{3}}\sqrt{\frac{W'(I)}{\mu}}\min\left(\frac{1}{\lambda_1},\frac{1}{\lambda_2}\right), \tag{2}$$

where λ_1 and λ_2 are the principal stretches in the plane of the thin layer, W is the elastic energy density, and $I = \lambda_1^2 + \lambda_2^2 + (\lambda_1\lambda_2)^{-2}$ is the first invariant of deformation [and hence, $\mu = 2W'(3)$]. For unconstrained films, the principal stretches are determined by the homogeneous solution; for constrained films, they are the fixed prestretches imposed prior to attachment to the rigid substrate. Above E_c, no stable configurations exist, neither homogeneous *nor* nonhomogeneous. As soon as E_c is attained, failure precursors appear, opening the way for a catastrophic failure of the film. The initial pattern of these precursors is a permanent signature for the subsequent inelastic processes; see Figs. 2 and 3.

To assess how formula (2) predicts the onset of catastrophic thinning, we first consider one-side constrained films for the creasing instability; see the sketch in the inset of Fig. 4.

For small stretches ($\lambda_1, \lambda_2 \leq 1.5$), the constitutive response can be modeled as neo-Hookean: $W = \mu(I-3)/2$, and formula (2) further simplifies to $E_c = \sqrt{2/3}\min(1/\lambda_1, 1/\lambda_2)$. Without prestretch ($\lambda_1 = \lambda_2 = 1$), this formula gives

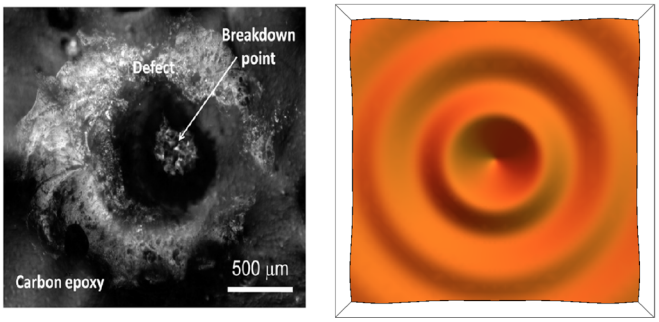

FIG. 2. (Left panel) Experimental creasing instability for non-prestretched one-side constrained films. Reprinted from [30], with the permission of AIP Publishing. (Right panel) Predicted failure precursor.

$E_c = \sqrt{2/3} = 0.816$, less than 4% off the value $E_c \simeq 0.85$ obtained experimentally [see Ref. [6], Fig. 3(b)] and closer than the estimate $E_c = 1.03$ obtained by FEM simulations [see Ref. [6], Fig. 4(b)]. For small values of uniaxial prestretch ($\lambda_1 = \lambda > 1$, $\lambda_2 = 1$), experiments [8] report an initial reduction of the critical electric field, in agreement with the prediction of formula (2) here, $E_c = \sqrt{2/3}\lambda^{-1}$. Beyond this initial negative effect, larger values of prestretch were measured as beneficial in increasing the critical electric field [8,9], an effect that has not yet been explained theoretically or numerically. To demonstrate the ability of formula (2) to reproduce this effect, we use a material model W which accounts for the strain stiffening induced by the limit chain extensibility of the elastomer in large deformations. Figure 4 shows the good agreement reached between our theory and the experiments (see the Supplemental Material [15] for the calibration of the model).

We then consider unconstrained films to study the onset of the pull-in instability; see the sketch in the inset of Fig. 5. For equibiaxially stretched films ($\lambda_1 = \lambda_2 = \lambda$) in the absence of dead loads, the homogeneous extension of the neo-Hookean elastomer is described by $E = \sqrt{\lambda^{-2} - \lambda^{-8}}$ (see Ref. [4] and the Supplemental Material

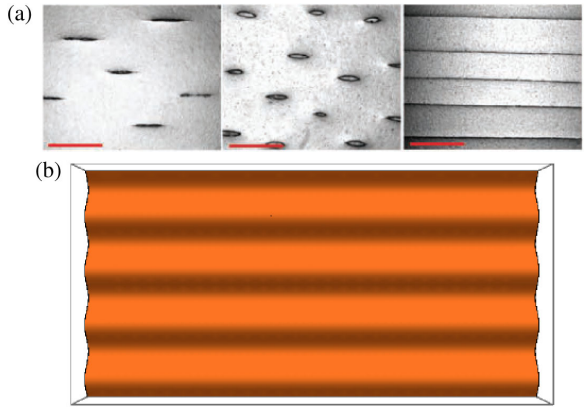

FIG. 3. (a) Alignment of creases in the direction of higher prestretch as voltage increases for one-side constrained films. Reprinted from [8], with the permission of John Wiley & Sons, Inc. (b) Failure precursors with $\lambda_1 = 2$, $\lambda_2 = 1$.

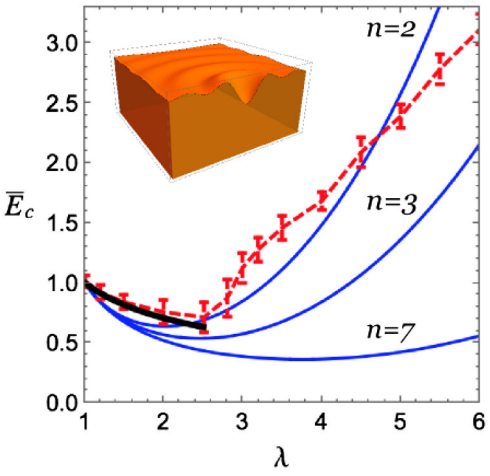

FIG. 4. Creasing instability after uniaxial prestretch. Comparison of experiments (the dashed line) [8] and theory (the solid curves, plotted for different values of n, the number of links in the Arruda-Boyce model). Here, $\bar{E}_c = E_c/\sqrt{2/3}$; see the Supplemental Material [15] for model calibration. A thick solid curve shows the previous qualitative trend based on dimensional or FEM analysis [8].

[15]). It reaches $E_c(\lambda) = \sqrt{2/3}\lambda^{-1}$ for $\lambda = 3^{1/6}$, where $E_c = \sqrt{2}/3^{2/3} = 0.680$, falling squarely within the range of the experimental values 0.678–0.686 in the absence of prestretch [5]. Thus, in the absence of dead loads, our analysis is close to the Hessian approach, which gives an estimate of $E_c = 0.687$ [4].

Things change drastically when the film is prestretched by applying dead loads prior to the voltage; then

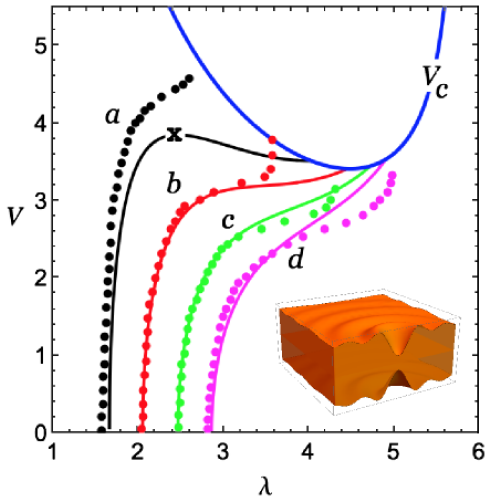

FIG. 5. Pull-in instability in equibiaxially strained films prestretched by dead loads. A comparison of experimental (dots) [7] and theoretical (solid curves) critical voltages (in kilovolts). Curves a, b, c, and d correspond to dead loads weighing 20, 25.5, 31, and 35.6 g, respectively: they describe homogeneous paths until failure and are modeled by the solid curves. Their intersection with the V_c curve [given by Eq. (2)] corresponds to catastrophic thinning (see the Supplemental Material [15] for details on the calibration). The Hessian approach can predict only one failure, denoted by x.

experiments show that *giant areal gains* can be achieved [7,31,32]. Theoretical models based on the Hessian approach fail to predict the actual gain, particularly for higher dead loads. That is because the Hessian criterion detects the points where the voltage-stretch curve ceases to be increasing [4]. However, elastomers stiffen greatly at large strains, and sufficiently high dead loads will make the voltage-stretch curve monotonically increasing: this phenomenon can lead to the erroneous conclusion that electromechanical instability can be eliminated by high prestretch, in contrast to experiments [7,33]. Consider, for example, experiments on voltage-actuated silicone disks, prestretched by dead loads, as carefully conducted and described in Ref. [7]. Based on the experimental results reported for the purely mechanical behavior of VHB™ silicone, we obtain the homogeneous loading curves for different values of dead loads using a strain-stiffening model [15]. For lower prestretches (Fig. 5), the voltage-stretch curves have a peak, corresponding to the failure resulting from the Hessian condition, but this peak disappears for higher values of prestretch, and the Hessian condition is no longer violated. Nonetheless, the experimental plots have a maximum, clearly corresponding to failure; see the last upper experimental dots in Fig. 5.

Our theory predicts failure whenever the homogeneous loading curves intersect the critical threshold curve described by formula (2). It gives a clear correspondence between the experimental and theoretical thresholds, as seen in Fig. 5.

We may thus conclude that the simple formula (2), coupled to that based on snap-through (Hessian) modeling [4,34], provides a complete picture of the electric breakdown experienced by unconstrained and one-side constrained voltage-actuated thin dielectrics; see the summary in Table I.

Our theory is based on energy minimization arguments [14]. *Stable* equilibrium configurations minimize the electroelastic free energy $\Psi = U - QV/2 - \mathcal{W}$, where U is the elastic energy, Q the total charge on the electrodes, V the voltage, and $\mathcal{W}$ the mechanical work [15], while surface energy terms are negligible [8]. When the membrane is thin and curvature effects are neglected [35], the electric field in the film can be approximated as $V/(h\lambda_3)$, where λ_3 is the thickness stretch. With these assumptions, the total free energy depends only on the deformation.

Thinness of the dielectric film leads to a Taylor expansion of Ψ in powers of h. Truncating $o(h^3)$ terms gives the minimal tools for detecting the onset of localization instabilities (higher-order terms are required for postcritical analysis, which is beyond the scope of this work). Denote by S the constrained (lower) surface for creasing, and the midsurface for pull-in. Then $\Psi = \int_S \psi da$, where the surface energy density ψ is expanded as

$$\psi(\lambda_i, \nabla\lambda_3) = h\varphi(\lambda_i) + h^3[\alpha_1(\lambda_i)\lambda_{3,1}^2 + \alpha_2(\lambda_i)\lambda_{3,2}^2]. \quad (3)$$

The stretches λ_i are functions of the planar coordinates (x_1, x_2), while the gradient $\nabla\lambda_3 = (\lambda_{3,1}, \lambda_{3,2})$ accounts for deformation inhomogeneities.

TABLE I. Experiments vs previous and present theories.

	Creasing			Pull-in				
Prestretch (dead load)	1	1–2.5	2.5–6	1	(20 g)	(25.5 g)	(31 g)	(36.5 g)
E_c [or V_c (kV)] experiments	0.85 [6]	✓ [8]	✓ [8]	0.678–0.686 [5]	✓ [7]	✓ [7]	✓ [7]	✓ [7]
E_c [or V_c (kV)] other theories	1.03 FEM [6]	x dim[a] [8]	x x	0.687 H[b] [4]	✓ H [7]	x x	x x	x x
E_c [or V_c (kV)] our theory	0.816	Fig. 4	Fig. 4	0.680	Fig. 5	Fig. 5	Fig. 5	Fig. 5

[a]For this stretch range only, a qualitative behavior was obtained in Ref. [8] through dimensional analysis.
[b]Hessian method.

When higher-order terms are not considered, only homogeneous configurations can be described. They are characterized by the Euler-Lagrange equations $\partial\varphi/\partial\lambda_i = 0$ and their stability is assessed through the convexity of φ, which is the so-called Hessian approach [4,34]. When applied to pull-in, this approach cannot predict instability, neither for nonequibiaxial states of deformation nor for large deformations [7]. When applied to creasing (for undeformed or prestretched films), it predicts stability for any voltage, which is clearly contradicted by the experiments.

These shortcomings are addressed by considering the whole energy (3), which imposes more stringent requirements for the existence of minimizers. Indeed, they exist provided that ψ is convex in $\nabla\lambda_3$, meaning that the functions α_1 and α_2 must both be positive. This is the case as long as the electric field is less than the critical threshold E_c defined by (2) [15].

Above E_c, the total free energy becomes concave in $\nabla\lambda_3$ and no energy minimizers exist (be they homogeneous or belonging to a wide class of nonhomogeneous ones). Immediately above E_c, inhomogeneous *failure precursors* become possible: as soon as they appear, they are energetically more favorable than the homogeneous state since they lower the total free energy, albeit without finding a minimum (Fig. 6): this explains the *catastrophic nature* of localized thinning. Experiments on one-side constrained films show that, when the film is not prestretched, localization mainly takes place in circular spots, whereas, when the film is prestretched in one direction prior to bonding to the rigid substrate, the resulting thinning localizations align in the direction of higher prestretch [8]; see Figs. 2 and 3. Both findings are easily covered by our theory.

Indeed, linearizing the Euler-Lagrange equation based on Eq. (3), we find that failure precursors of the type $\lambda_3(x_1, x_2) = \lambda_3^o + w(x_1, x_2)$, with λ_3^o being a constant and w small, solve [15]

$$\alpha_1 w_{,11} + \alpha_2 w_{,22} - \Gamma w = 0, \tag{4}$$

where α_1, α_2, and Γ are functions of the underlying stretch and the electric field. For almost incompressible materials, Γ is always positive, whereas, as we have seen, α_1 and α_2 become negative above the critical voltage defined by Eq. (2). For undeformed or equibiaxially stretched layers, $\alpha_1 = \alpha_2$, and they become negative together for $E > E_c$, meaning that polar symmetric solutions of the Bessel type become possible; see Fig. 2. When the film is prestretched with $\lambda_1 > \lambda_2$, for example, the first coefficient that becomes negative is α_2, leading to sinusoidal solutions in the direction of least stretch; see Fig. 3.

With this Letter, we improved the current understanding of the catastrophic nature of electroelastic instabilities in thin films. This unsolved problem goes back as early as 1880, when Röntgen [33] stretched natural rubber using sprayed-on electric charges. In 1955, Stark and Garton [36] detected a previously unrecognized form of breakdown due to the mechanical deformation of electrically irradiated thin films of cross-linked polythane. The first experimental

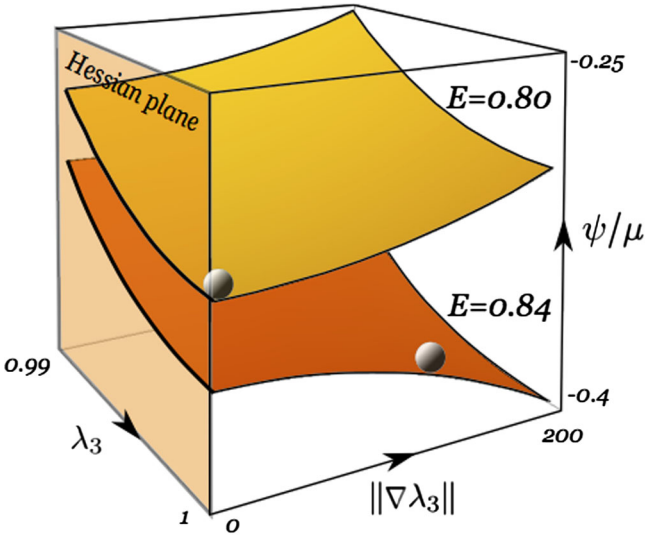

FIG. 6. Electroelastic free energy ψ/μ for a one-side constrained film without prestretch ($\lambda_1 = \lambda_2 = 1$). The film is a slightly compressible neo-Hookean material of thickness $h = 0.01L$, where L is a typical lateral length scale and $\kappa/\mu = 1000$, with κ being the initial bulk modulus [see Eqs. (7) and (8) in the Supplemental Material [15]]. For $E < E_c = 0.816$, the homogeneous solution with $\lambda_3 = 1$ is the unique energy minimizer; see the upper surface. Above E_c, the energy is still convex in λ_3, but it becomes nonconvex in $\nabla\lambda_3$; see the lower surface. Failure precursors are then energetically favored, but no energy minimizers exist. In the shaded *Hessian plane* (at $\|\nabla\lambda_3\| = 0$), Hessian stability takes place; there, the energy is convex in λ_3 and the failure threshold cannot be captured.

evidence that dielectric breakdown is due to strong thinning localization was by Blok and LeGrand 1 in 1969, who provided clear optical evidence (Fig. 1) in voltage-controlled polymer films. They speculated that it is experimentally impossible to deform the entire area of the dielectric without using an immense stress, thus inferring the energetic convenience of localizing deformations above a critical voltage. Here, we further their intuition and find a completely new paradigm for the analysis of electromechanical instabilities in dielectric films, both one-side constrained and unconstrained. A great majority of technological applications based on dielectric elastomers are dependent on whether wrinkling may or may not be anticipated by electromechanical instability, e.g., tunable adhesion, open-channel microfluidics, etc. [37,38], and on-demand fluorescent patterning [39]. By redefining and furthering the concept of the electromechanical instability of dielectric films, this Letter implies that new experimental campaigns and new analytical studies based on formula (2) are now required to generate a finer physical picture of the catastrophic thinning phenomenon.

Authors acknowledge funding from Italian Ministry MIUR-PRIN voce COAN 5.50.16.01 code 2015JW9NJT.

*giuseppe.zurlo@nuigalway.ie

[1] R. E. Pelrine, R. D. Kornbluh, Q. Pei, and J. P. Joseph, High-speed electrically actuated elastomers with strain greater than 100%, Science **287**, 836 (2000).
[2] J. Huang, S. Shian, R. M. Diebold, Z. Suo, and D. R. Clarke, The thickness and stretch dependence of the electrical breakdown strength of an acrylic dielectric elastomer, Appl. Phys. Lett. **101**, 122905 (2012).
[3] J. Blok and D. G. LeGrand, Dielectric breakdown of polymer films, J. Appl. Phys. **40**, 288 (1969).
[4] X. Zhao and Z. Suo, Method to analyze electromechanical stability of dielectric elastomers, Appl. Phys. Lett. **91**, 061921 (2007).
[5] R. E. Pelrine, R. D. Kornbluh, and J. P. Joseph, Electrostriction of polymer dielectrics with compliant electrodes as a means of actuation, Sens. Actuators A **64**, 77 (1998).
[6] Q. Wang, L. Zhang, and X. Zhao, Creasing to Cratering Instability in Polymers under Ultrahigh Electric Fields, Phys. Rev. Lett. **106**, 118301 (2011).
[7] J. Huang, T. Li, C. C. Foo, J. Zhu, D. R. Clarke, and Z. Suo, Giant, voltage-actuated deformation of a dielectric elastomer under dead load, Appl. Phys. Lett. **100**, 041911 (2012).
[8] Q. Wang, M. Tahir, J. Zang, and X. Zhao, Dynamic electrostatic lithography: Multiscale on-demand patterning on large-area curved surfaces, Adv. Mater. **24**, 1947 (2012).
[9] Q. Wang, M. Tahir, J. Zang, and X. Zhao, Electro-creasing instability in deformed polymers: Experiment and theory, Soft Matter **7**, 6583 (2011).
[10] K. Bertoldi and M. Gei, Instabilities in multilayered soft dielectrics, J. Mech. Phys. Solids **59**, 18 (2011).
[11] D. De Tommasi, G. Puglisi, and G. Zurlo, Inhomogeneous deformations and pull-in instability in electroactive polymeric films, Int. J. Nonlinear Mech. **57**, 123 (2013).
[12] L. Dorfmann and R. W. Ogden, *Nonlinear Theory of Electroelastic and Magnetoelastic Interactions* (Springer, New York, 2014).
[13] G. Zurlo, Non-local elastic effects in electroactive polymers, Int. J. Nonlinear Mech. **56**, 115 (2013).
[14] D. De Tommasi, G. Puglisi, and G. Zurlo, Electromechanical instability and oscillating deformations in electroactive polymer films, Appl. Phys. Lett. **102**, 011903 (2013).
[15] See Supplemental Material at http://link.aps.org/supplemental/10.1103/PhysRevLett.118.078001, which includes Refs. [16–29], for details on the derivation and calibration of the model.
[16] B. Audoly and J. W. Hutchinson, Analysis of necking based on a one-dimensional model, J. Mech. Phys. Solids **97**, 68 (2016).
[17] E. M. Arruda and M. C. Boyce, Three-dimensional constitutive model of the large stretch behavior of rubber elastic materials, J. Mech. Phys. Solids **41**, 389 (1993).
[18] B. D. Coleman and D. C. Newman, On the rheology of cold drawing. I. Elastic materials, J. Polym. Sci., Part B: Polym. Phys. **26**, 1801 (1988).
[19] B. Dacorogna, *Introduction to the Calculus of Variations* (Imperial College Press, London, 2004).
[20] D. DeTommasi, G. Puglisi, and G. Zurlo, Electromechanical instability and oscillating deformations in electroactive polymer films, Appl. Phys. Lett. **102**, 011903 (2013).
[21] D. DeTommasi, G. Puglisi, and G. Zurlo, Inhomogeneous deformations and pull-in instability in electroactive polymeric films, Int. J. Nonlinear Mech. **57**, 123 (2013).
[22] D. DeTommasi, G. Puglisi, and G. Zurlo, Failure modes in electroactive polymer thin films with elastic electrodes, J. Phys. D **47**, 065502 (2014).
[23] R. Fosdick and H. Tang, Electrodynamics and thermomechanics of material bodies, J. Elast. **88**, 255 (2007).
[24] A. N. Gent, A new constitutive relation for rubber, Rubber Chem. Technol. **69**, 59 (1996).
[25] W. Hong, Modeling viscoelastic dielectrics, J. Mech. Phys. Solids **59**, 637 (2011).
[26] C. Miehe, D. Vallicotti, and S. Teichtmeister, Homogenization and multiscale stability analysis in finite magneto-electro-elasticity, GAMM-Mitt. **38**, 313 (2015).
[27] R. W. Ogden, G. Saccomandi, and I. Sgura, On worm-like chain models within the three-dimensional continuum mechanics framework, Proc. R. Soc. A **462**, 749 (2006).
[28] T. J. Pence and K. Gou, On compressible versions of the incompressible neo-Hookean material, Math. Mech. Solids **20**, 157 (2015).
[29] G. Zurlo, Mathematisches Forschungsinstitut Oberwolfach Report No. 49, 2015.
[30] L. Zhang, Q. Wang, and X. Zhao, Mechanical constraints enhance electrical energy densities of soft dielectrics, Appl. Phys. Lett. **99**, 171906 (2011).
[31] L. Jiang, A. Betts, D. Kennedy, and S. Jerrams, Eliminating electromechanical instability in dielectric elastomers by employing pre-stretch, J. Phys. D **49**, 265401 (2016).
[32] B. Li, H. Chen, J. Qiang, S. Hu, Z. Zhu, and Y. Wang, Effect of mechanical pre-stretch on the stabilization of

dielectric elastomer actuation, J. Phys. D **44**, 155301 (2011).

[33] C. Keplinger, M. Kaltenbrunner, N. Arnold, S. Bauer, and A. Röntgen, Electrode-free elastomer actuators without electromechanical pull-in instability, Proc. Natl. Acad. Sci. U.S.A. **107**, 4505 (2010).

[34] A. N. Norris and Comment on, Method to analyze electromechanical stability of dielectric elastomers, Appl. Phys. Lett. **92**, 026101 (2008).

[35] G. Puglisi and G. Zurlo, Electric field localizations in thin dielectric films with thickness non-uniformities, J. Electrost. **70**, 312 (2012).

[36] K. H. Stark and C. G. Garton, Electric strength of irradiated polythene, Nature (London) **176**, 1225 (1955).

[37] S. Yang, K. Khare, and P.-C. Lin, Harnessing surface wrinkle patterns in soft matter, Adv. Funct. Mater. **20**, 2550 (2010).

[38] Y. Cao and J. W. Hutchinson, Wrinkling phenomena in neo-Hookean film/substrate bilayers, J. Appl. Mech. **79**, 031019 (2012).

[39] Q. Wang, G. R. Gossweiler, S. L. Craig, and X. Zhao, Cephalopod-inspired design of electro-mechano-chemically responsive elastomers for on-demand fluorescent patterning, Nat. Commun. **5**, 4899 (2014).

Supplementary material

Model derivation

Thermodynamical considerations for electro-elastic materials undergoing relatively slow motions lead to a formulation of electro-elastic equilibrium as a minimisation problem for a suitable *total free energy* functional [8, 10, 13]. The undeformed configuration of the electro-elastic film is a flat prismatic plate R with uniform cross section and thickness h, which we assume small relative to the diameter L of the membrane. For simplicity we set $L = 1$ so that $h \equiv h/L \ll 1$ takes the role of a *smallness parameter*. The lower electrode is assumed to be at zero voltage and the upper electrode at voltage V. Our analysis is valid for 'ideal dielectric elastomers' [19], for which the polarisation is fluid-like and independent of the deformation. Under these assumptions, when voltage is fixed the total free energy takes the form

$$\hat{\Psi}(\mathbf{f}, \tilde{\mathbf{d}}) = U(\mathbf{f}) - \frac{V\,Q(\mathbf{f}, \tilde{\mathbf{d}})}{2} - \mathscr{W}(\mathbf{f}), \tag{1}$$

where U is the free elastic energy, $\mathbf{f}$ the film deformation, $\tilde{\mathbf{d}}$ the (Lagrangian) electric displacement, Q the total charge on the upper electrode and $\mathscr{W}$ the work of mechanical forces on the film edges.

When the film thickness is small, we find approximated solutions $\tilde{\mathbf{d}}_\mathbf{f}$ to the electro-static problem for arbitrary deformations, and the total free energy can be recast as

$$\Psi(\mathbf{f}) = \hat{\Psi}(\mathbf{f}, \tilde{\mathbf{d}}_\mathbf{f}) = U(\mathbf{f}) - \frac{Q(\mathbf{f}, \tilde{\mathbf{d}}_\mathbf{f})\,V}{2} - \mathscr{W}(\mathbf{f}). \tag{2}$$

Now the problem can be formulated in the familiar framework of classical elasticity, where deformation is the only unknown. To capture inhomogeneous thinning we minimise the energy (2) over an approximated class of deformations [3] bringing a point $\boldsymbol{x} \in R$ to the current position

$$\mathbf{f}(\boldsymbol{x}) = \mathbf{g}(x_1, x_2) + \lambda_3(x_1, x_2) x_3 \boldsymbol{i}_3, \tag{3}$$

where $\mathbf{g}$ describes the planar component of deformation, perpendicular to the thickness direction $\boldsymbol{i}_3$, and where λ_3 is the thickness stretch. We have $-h/2 \le x_3 \le h/2$ for unconstrained films and $0 \le x_3 \le h$ for one-side constrained films. In both cases we denote by S the surface $x_3 = 0$.

The gradient of the deformation (3) is

$$\mathbf{F} = \nabla \mathbf{f} = \mathbf{G} + \lambda_3 \boldsymbol{i}_3 \otimes \boldsymbol{i}_3 + x_3 \boldsymbol{i}_3 \otimes \nabla \lambda_3, \tag{4}$$

where $\mathbf{G} = \nabla \mathbf{g}$ is the in-plane deformation tensor, which may be recast as $\mathbf{G} = \lambda_1 \boldsymbol{i}_1 \otimes \boldsymbol{i}_1 + \lambda_2 \boldsymbol{i}_2 \otimes \boldsymbol{i}_2$ with $\boldsymbol{i}_1 \perp \boldsymbol{i}_2$ both perpendicular to $\boldsymbol{i}_3$ and where λ_1, λ_2 are the planar principal stretches. Volume variations are measured by $J = \det \mathbf{F} = \lambda_1 \lambda_2 \lambda_3$, so that incompressibility requires $\lambda_1 \lambda_2 \lambda_3 = 1$. Observe that if the film were exactly incompressible and, as in the case of one-side constrained film, the principal stretches λ_1 and λ_2 are fixed before gluing the membrane to the rigid electrode, it would follow that $\lambda_3 = (\lambda_1 \lambda_2)^{-1}$ must be constant, and no further deformations may take place in the class (3). To describe creasing deformations we relax this constraint by taking a strain energy density for slightly compressible materials, separating the volumetric from the deviatoric part as follows [15],

$$\overline{W} = W\left(I/J^{-2/3}\right) + \kappa\,\Phi(J), \tag{5}$$

where $I = \mathrm{tr}(\mathbf{F}^T\mathbf{F})$, $\Phi(J)$ is such that $\Phi(1) = \Phi'(1) = 0$, and κ is the *infinitesimal bulk modulus*. Then exact incompressibility is the limit $J \to 1$ and $\kappa/\mu \to \infty$ where $\mu = W'(3)$ is the infinitesimal shear modulus. The free energy stored in the plate can be calculated as $U = \int_S \int_b^c \overline{W}(\mathbf{F}(\boldsymbol{x}))\,dx_3\,dA$, where $dA = dx_1 dx_2$.

Regarding the electric part of the problem, the charge on the upper electrode is $Q = \int \sigma^+\,da^+$ where σ^+ is the charge density per unit area. Assuming that the external electric field is null, we have $\sigma^+ = \varepsilon \mathrm{e}^+$ where ε is the dielectric permittivity and e^+ the normal component of the Eulerian electric field on the upper electrode. Thanks to the film slenderness [16], we can neglect curvature effects on the electric field and we consider that $\mathrm{e}^+ \simeq \mathrm{e} \simeq V/(h\lambda_3)$. This approximation is consistent with nonlocal effects for the mechanical behaviour of the electrodes not having been taken into consideration [7, 20]. The surface stretch of the upper electrode is found from Nanson's formula as $da^+/dA = \|J\mathbf{F}^{-\mathsf{T}}\boldsymbol{i}_3\|_{x_3=c}$.

The work term only needs to be expressed when dealing with unconstrained films (for one-side constrained films we will consider the planar stretches, if any, to be fixed.) Denoting by s_1, s_2 the Lagrangian edge line stress components (force per undeformed length) of the membrane, we find

$$\mathscr{W} = h \int_S (s_1\lambda_1 + s_2\lambda_2)\,dA. \tag{6}$$

Since the film is slender we can perform a Taylor expansion of the total free energy (2) in powers of h, truncating $o(h^3)$ terms. After through-thickness integration, we thus obtain that $\Psi(\mathbf{f}) = \int_S \psi(\mathbf{F}(\boldsymbol{x}))\,dA$ where ψ is the surface free energy. Finally, we introduce the dimensionless electric field,

$$E = (V/h)\sqrt{\varepsilon/\mu}, \tag{7}$$

where μ is the *infinitesimal shear modulus*.

For *one-side constrained* films, we consider λ_1, λ_2 to be homogeneous and prescribed by the pre-stretching of the film prior to attaching it to the rigid substrate. The film is not exactly incompressible, so λ_3 is the independent variable. We thus obtain [21]

$$\psi(\lambda_3, \nabla\lambda_3) = h\varphi(\lambda_3) + h^3\left[\alpha_1(\lambda_3)\lambda_{3,1}^2 + \alpha_2(\lambda_3)\lambda_{3,2}^2\right], \tag{8}$$

where $\lambda_{3,i} = \partial\lambda_3/\partial x_i$ and

$$\begin{aligned}\varphi &= W(I/J^{2/3}) + \kappa\,\phi(J) - \mu E^2 j/(2\lambda_3),\\ \alpha_1 &= 4J^{1/3}W'(I/J^{2/3}) - 3\mu E^2\lambda_2^2,\\ \alpha_2 &= 4J^{1/3}W'(I/J^{2/3}) - 3\mu E^2\lambda_1^2.\end{aligned} \tag{9}$$

Here, $I = \lambda_1^2+\lambda_2^2+\lambda_3^2$ and $j = \lambda_1\lambda_2$ (which is fixed).

For *unconstrained* films, we impose exact incompressibility ($\lambda_3 = 1/j$), and then

$$\psi(\lambda_i, \nabla\lambda_3) = h\varphi(\lambda_i) + h^3\left[\alpha_1(\lambda_i)\lambda_{3,1}^2 + \alpha_2(\lambda_i)\lambda_{3,2}^2\right], \tag{10}$$

where $i = 1, 2$ and

$$\begin{aligned}\varphi &= W(I) - \mu E^2 j^2/2 - s_1\lambda_1 - s_2\lambda_2,\\ \alpha_1 &= \left[4W'(I) - 3\mu E^2\lambda_2^2\right]/48,\\ \alpha_2 &= \left[4W'(I) - 3\mu E^2\lambda_2^1\right]/48.\end{aligned} \tag{11}$$

Here, $I = \lambda_1^2+\lambda_2^2+(\lambda_1\lambda_2)^{-2}$. Note that for equi-biaxially stretched films, $\lambda_1 = \lambda_2 = \lambda_3^{-1/2} = \lambda$, say.

Energy minimisation

Here we exploit known necessary conditions for the existence of minimisers from direct methods of calculus of variations [4]. Assessing these necessary conditions does not rely on finding explicit nontrivial solutions but rather on direct inspection of the energy.

Consider a scalar function $u(\boldsymbol{x}) : S \subset \mathbb{R}^2 \to \mathbb{R}$ with $u = u_0$ prescribed on the edge ∂S and consider the energy functional

$$\Psi(u) = \int_S \psi(\boldsymbol{x}, u(\boldsymbol{x}), \nabla u(\boldsymbol{x}))\, dA. \tag{12}$$

According to direct methods of calculus of variations [4], *minimisers* of Ψ exist provided that:

(h1) $\boldsymbol{\xi} \to \psi(\bullet, \bullet, \boldsymbol{\xi})$ is convex,

(h2) there exist $p > q \geq 1$ and $a_1 > 0$, $a_2, a_3 \in \mathbb{R}$ such that $\psi(\boldsymbol{x}, u, \boldsymbol{\xi}) \geq a_1\|\boldsymbol{\xi}\|^p + a_2\|u\|^q + a_3$ for all $(\boldsymbol{x}, u, \boldsymbol{\xi})$.

Uniqueness of minimizers of $I(u)$ holds provided that

(h3) $(u, \boldsymbol{\xi}) \to \psi(\bullet, u, \boldsymbol{\xi})$ is strictly convex

Condition (h3) implies (h1)-(h2). Candidate minimisers of $I(u)$ must be sought among the stationary solutions of the functional $\Psi(u)$, found from the Euler-Lagrange equations

$$\frac{\partial\psi}{\partial u} = \mathrm{Div}\left(\frac{\partial\psi}{\partial\nabla u}\right) \qquad u = u_o \ \text{ on } \ \partial S. \tag{13}$$

Our main achievement here is to show that electromechanical instability corresponds to violation of the condition (h1).

Observe that Hessian approach consist in checking the convexity of ψ in u, which is not a necessary condition for the existence of minimisers but is rather related to condition (h3), hence to uniqueness.

Analysis of creasing for one-side constrained films

Here the prescribed pre-streches λ_1, λ_2 are homogeneous and the only unknown is the function λ_3. Homogeneous configurations λ_3^0 are found by solving the algebraic equation $\partial\varphi/\partial\lambda_3 = 0$. Note that or large κ the material is almost incompressible and $\lambda_3^0 \simeq (\lambda_1\lambda_2)^{-1}$.

A necessary condition for λ_3^0 to be a minimiser of $\Psi(\lambda_3)$ is that (h1) holds. It is immediate to check that this condition is satisfied as long as the functions α_1, α_2 of $(8)_{2\text{–}3}$ are positive, that is as long as

$$E < E_c = \frac{2}{\sqrt{3}}\sqrt{\frac{W'(I/J^{2/3})}{\mu}}\,\frac{\lambda_3}{J^{5/6}}\min(\lambda_1, \lambda_2), \tag{14}$$

where I, J are evaluated at $\lambda_1, \lambda_2, \lambda_3^0$. In the exact incompressibility limit the critical electric field above tends to

$$\boxed{E_c = \frac{2}{\sqrt{3}}\sqrt{\frac{W'(I)}{\mu}}\min\left(\frac{1}{\lambda_1}, \frac{1}{\lambda_2}\right),} \tag{15}$$

which is our main finding. We show below that this threshold is the same for unconstrained incompressible films. If the function $\psi(\lambda_3, \nabla\lambda_3)$ is strictly convex in both arguments, then the homogeneous solution λ_3^0 is also unique under homogeneous boundary conditions, according to (h3).

As soon as (h1) is violated the energy functional $\Psi(\lambda_3)$ no longer admits minimisers in the class of deformations (3); in particular, homogeneous configurations cannot be energy minimisers. Observe that this conclusion holds even if (h1) is violated while $\psi(\lambda_3, \bullet)$ is still convex in λ_3, which means that our condition is more restrictive than the positivity of the Hessian condition. Clearly, violation of (h1) does not exclude that other inhomogeneous solutions may exist outside the class (3); nonetheless, we can show that immediately above E_c inhomogeneous *failure precursors* become possible within the class (3), that can lower the energy below $\Psi(\lambda_3^0)$, although the energy density has no minima beyond this threshold. For this reason we call these failure precursors *catastrophic*.

To find out what these inhomogeneous precursors look like at their onset and to shed light on the physics of the problem, we consider a specific form for the strain energy density, the compressible neo-Hookean material [15] with $W(I) = \mu(I/J^{2/3} - 3)/2$ and $\phi(J) = (J^2 + J^{-2} - 2)/8$, and we look for inhomogeneous solutions $\lambda_3(\boldsymbol{x}) = \lambda_3^0 + w(\boldsymbol{x})$ with w small and $\lambda_3^o \simeq 1/(\lambda_1\lambda_2)$. The equation for w is then

$$\lambda_2^2\left(E^2 - \frac{2}{3}\frac{1}{\lambda_2^2}\right)w_{,11} + \lambda_1^2\left(E^2 - \frac{2}{3}\frac{1}{\lambda_1^2}\right)w_{,22} + \frac{\Gamma}{h^2}w = 0, \tag{16}$$

where $\Gamma = \left[16 + \lambda_1^2\lambda_2^2\left(6\kappa/\mu - 4\lambda_1^2 - 4\lambda_2^2 + 5\lambda_1^2\lambda_2^2E^2\right)\right]/3$. To find out whether non-trivial solutions are possible, first observe that for nearly incompressible materials

($\kappa/\mu \gg 1$), Γ is positive for all values of pre-stretch. Furthermore, the coefficients of $w_{,11}$ and $w_{,22}$ remain negative as long as $E < E_c$, meaning that no bounded, non-trivial, real solutions exist below this threshold; this clearly agrees with our general findings. However, as soon as one (or both) of the coefficients becomes positive, non-trivial solutions exist; this happens precisely when (h1) is violated.

In the absence of pre-stretch ($\lambda_1 = \lambda_2 = 1$), we find radial solutions of the form

$$w(\varrho) = CJ_0\left(\frac{\omega\varrho}{h}\right), \qquad \varrho = \sqrt{x_1^2 + x_2^2}, \tag{17}$$

where J_0 is the Bessel function of the first kind, $\omega = \sqrt{\Gamma/(E^2 - 2/3)}$ and C is an undetermined amplitude coefficient. In the presence of pre-stretch, experiments show that periodic creases appear perpendicularly to the direction of highest pre-stretch. When $\lambda_1 > \lambda_2$, say, as soon as the electric field falls within the range $\sqrt{2/3}/\lambda_1 < E < \sqrt{2/3}/\lambda_2$, the coefficient of $w_{,22}$ becomes positive while the coefficient of $w_{,11}$ remains negative, meaning that periodic solutions of the form

$$w(x_1, x_2) = C_1 \cos\left(\omega\,\frac{x_2}{h}\right) + C_2 \sin\left(\omega\frac{x_2}{h}\right) \tag{18}$$

become possible, where $\omega = \sqrt{\Gamma/(E^2 - E_c^2)}/\lambda_1$ and C_1, C_2 are constants. Here the mechanical interpretation is that periodic patterns will become possible in the direction of least stretch, whereas in equi-biaxially stretched dielectrics there is no preferential direction and polar symmetric solutions may be attained; this agrees with experiments.

Observe that, for both types of precursors presented above, the period of the failure precursors tends to zero at the onset of instability and increases immediately above the critical voltage. It the context of pull-in instability analysis, it was shown that this effect may be regularised by taking into consideration non-local effects [5–7, 16, 20]. However, observe that discussing the nature of the post-critical shape of creases is beyond the limits of our simplified treatment for precursors. Furthermore, due to the limited deformation mode which is permitted by the ansatz, the prediction from the present analysis may be considered an upper bound of the critical electrical field. A more refined analysis certainly requires a wider class of deformations [1], together with higher-order effects for both the electrical and mechanical behaviour of the electrode.

Calibration of the Arruda-Boyce model for creasing

We calibrated the 5-term Arruda and Boyce [2] model to reproduce the experimental results reported in [17] as follows. First we use the Arruda-Boyce truncated strain energy density

$$W(I) = \mu_0\left[\frac{I-3}{2} + \frac{I^2-9}{20\,n} + \frac{11(I^3-27)}{1050\,n^2} + \frac{19(I^4-81)}{7000\,n^3} + \frac{519(I^5-243)}{673750\,n^4}\right], \tag{19}$$

where n is the number of links in the 8-chain model. Note that in (19) $\mu_0 \neq 2W'(3)$, i.e. μ_0 is not the infinitesimal shear modulus (in fact, $\mu = 2W'(3) = \mu_0[1 + 3/(5n) + 99/(175n^2) + 513/(875n^3 + 42039/(67375n^4)]$). We then specialise the general equation (15) to a uniaxial pre-stretch as described in [17], so that $\lambda_1 = \lambda$, $\lambda_2 = \lambda_3 = \lambda^{-1/2}$, and $I = \lambda^2 + 2\lambda^{-1}$. When $\lambda = 1$, Wang et al. [17] gave $E_c = 1$ instead of their measured [18] value $E_c = 0.85$, meaning that they normalised their critical electric field–stretch curve with respect to that value. To model their data we thus have to calibrate our formula (15) with respect to its first value $E_c = \sqrt{2/3} = 0.816$ at $\lambda = 1$. Then we show the curves found when the parameter n varies from 2 to 7, indeed a realistic range for silicone materials used in electro-patterning applications, see Fig.4 in the main paper.

Analysis of pull-in for unconstrained films

The analysis here follows the same path as for creasing instability. Confining attention to equi-biaxially pre-stretched configurations under the action of equal edge dead-loads, so that $\lambda_1 = \lambda_2 = \lambda_3^{-1/2} = \lambda$ and $s_1 = s_2 = s$, we obtain the general solution for the homogeneous loading branches by solving $\partial\varphi/\partial\lambda = 0$ as

$$E^0(\lambda) = \sqrt{\frac{2(\lambda^{-2} - \lambda^{-8})W'(I) - s\lambda^{-3}}{\mu}}, \tag{20}$$

where $I = 2\lambda^2 + \lambda^{-4}$. It is straightforward to check that also in this case the necessary condition for the existence of minimisers coincides with (15). Its specialisation to the equi-biaxial case is trivial:

$$E_c = \frac{2}{\sqrt{3}}\sqrt{\frac{W'(I)}{\mu}}\frac{1}{\lambda}. \tag{21}$$

For the analysis of failure precursors, the same treatment as that for creasing holds, and we do not repeat it for brevity. In this case the critical points are determined by the intersections of the E_0 curve with the E_c curve. These expressions are used in the main paper (Fig.5) to capture the data of Wang et al. [11] (see below for the calibration of the model).

Our formula also works when the extension is not equi-biaxial extension, a case where the Hessian approach also reveals its limitations. Take a neo-Hookean dielectric film where $\lambda_1 > 1$ is fixed and a traction s_2 is applied in direction $\boldsymbol{i}_2$. Here the homogeneous configuration is retrieved

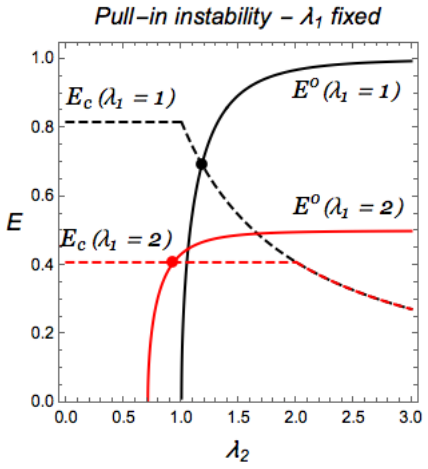

FIG. 1. Voltage versus λ_2 with λ_1 fixed. Intersection of the solid and dashed curves gives the upper voltage thresholds in both cases.

from $\partial\varphi/\partial\lambda_2 = 0$, giving

$$E^0(\lambda_2) = (\lambda_1\lambda_2)^{-2}\sqrt{\lambda_1^2\lambda_2^3(\lambda_2 - s_2/\mu) - 1}. \qquad (22)$$

We then find that along this homogenous loading curve, $\varphi''(\lambda_2) = 1+3\lambda_1^{-2}\lambda_2^{-4}-(E^0)^2\lambda_1^2 \geq 0$, with equality holding only for $\lambda_2 \to \infty$. Hence, according to the Hessian approach, failure occurs at infinite stretch, which is clearly unrealistic. On the other hand, formula (15) gives values of $E_c(\lambda_2)$ for each value of λ_1, represented by dashed curves in Fig.1. The intersection of that curve with the curve of E^0 then gives the critical voltage for any pre-stretch.

Model calibration for pull-in

Tuning of the constitutive model with the experimental data provided in [11] was done directly on the lower frequency voltage-stretch curves, where viscoelastic effects are less relevant. The following Worm-Like Chain modification of the Gent model [14]

$$W(I) = \mu\frac{1+b}{1+2b}J_m \ln\left(\frac{b}{1+b}\frac{I-3}{J_m-(I-3)} + \frac{J_m}{J_m-(I-3)}\right), \qquad (23)$$

was used to obtain a best fit of the homogeneous loading curves. Here the best simultaneous fit for the four homogeneous loading curves was obtained with $b = -5$, $J_m = 65$ and $\mu = 20.5$ kPa.

[1] Audoly B., Hutchinson J.W., Analysis of necking based on a one-dimensional model, J. Mech. Phys. Solids, in press (2016) doi: 10.1016/j.jmps.2015.12.018

[2] Arruda E.M., Boyce M.C., Three-dimensional constitutive model of the large stretch behavior of rubber elastic materials, J. Mech. Phys. Solids, 41, 389–412 (1993).

[3] Coleman B.D., Newman D. C., On the rheology of cold drawing. I. Elastic materials, J. Polym. Sci.: Part B: Polym. Phys. 26, 1801–1822 (1988).

[4] Dacorogna B., Introduction to the calculus of variations, Imperial College Press (2004).

[5] DeTommasi D., Puglisi G., Zurlo G., Electromechanical instability and oscillating deformations in electroactive polymer films, Appl. Phys. Lett., 102, 011903 (2013).

[6] DeTommasi D., Puglisi G., Zurlo G., Inhomogeneous deformations and pull-in instability in electroactive polymeric films, Int. J. Non-Lin. Mech., 57, 123–129 (2013).

[7] DeTommasi D., Puglisi G., Zurlo G., Failure modes in electroactive polymer thin films with elastic electrodes, J. Phys. D: Appl. Phys. 47 065502 (2014).

[8] Fosdick R., Tang H., Electrodynamics and thermomechanics of material bodies, J. Elasticity 88, 255–297 (2007).

[9] Gent A. N., A new constitutive relation for rubber. Rubber Chem. Technol. 69, 59–61 (1996).

[10] Hong W., Modeling viscoelastic dielectrics, J. Mech. Phys. Solids 59, 637–650 (2011).

[11] Huang J., Li T. , Chiang Foo C., Zhu J., Clarke D.R., Suo Z., Giant, voltage-actuated deformation of a dielectric elastomer under dead load, Appl. Phys. Lett. 100, 041911 (2012).

[12] Li B., Chen H., Qiang J., Hu S., Zhu Z., Wang Y., Effect of mechanical pre-stretch on the stabilization of dielectric elastomer actuation, J. Phys. D: Appl. Phys. 44, 155301 (2011).

[13] Miehe C., Vallicotti D., Teichtmeister S., Homogenization and multiscale stability analysis in finite magneto-electro-elasticity, GAMM-Mitt. 38, No. 2, 313–343 (2015).

[14] Ogden R.W., Saccomandi G., Sgura I., On worm-like chain models within the three-dimensional continuum mechanics framework, Proc. R. Soc. A, 462, 749–768 (2006).

[15] Pence T.J., Gou K., On compressible versions of the incompressible neo-Hookean material, Mathematics and Mechanics of Solids, 1–26, (2014).

[16] Puglisi G., Zurlo G., Electric field localizations in thin dielectric films with thickness non-uniformities, J. Electrostatics, 70(3), 312–316 (2012).

[17] Wang Q., Tahir M., Zang J., Zhao X., Dynamic electrostatic lithography: multiscale on-demand patterning on large-area curved surfaces, Adv. Mater., 24, 1947–1951 (2012).

[18] Wang Q., Zhang L., Zhao X. Creasing to cratering instability in polymers under ultrahigh electric fields. Phys. Rev. Lett. 106, 118301 (2011).

[19] Zhao X., Suo Z., Method to analyze electromechanical stability of dielectric elastomers. Appl. Phys. Letters, 91 (2007) 061921.

[20] Zurlo G., Non-local elastic effects in electroactive polymers, Int. J. Non.linear Mech. 56, 115–122 (2013).

[21] Zurlo, G., Mathematisches Forschungsinstitut Oberwolfach, Report No. 49 (2015) doi: 10.4171/OWR/2015/49